Supplement

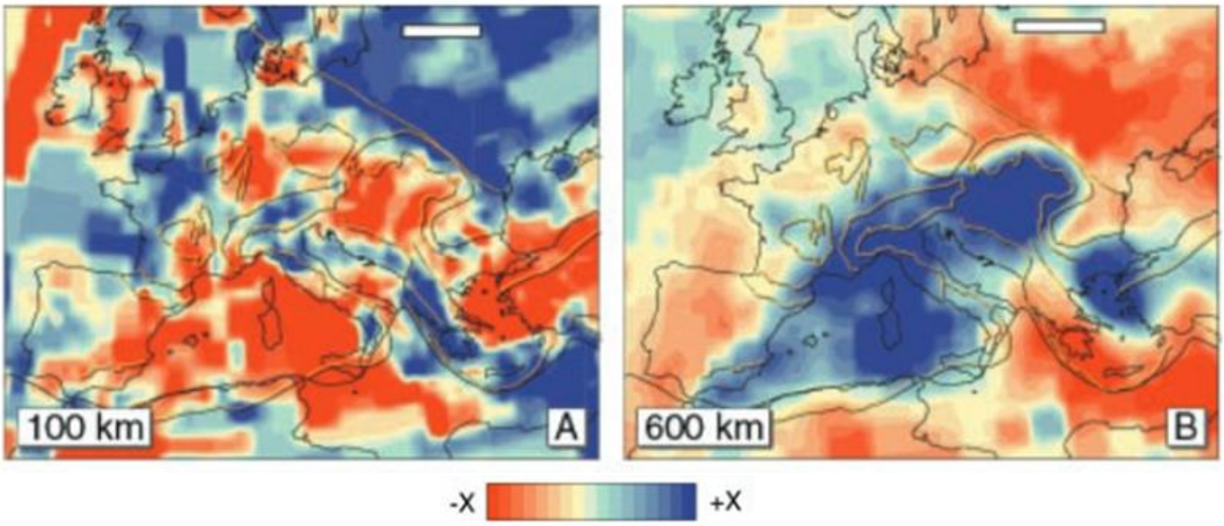

Figure S1 from Goes et al. (1999): Tomographic images of P-wave velocity anomalies represented as deviations from a one-dimensional reference model [AK135, (Kennett et al., 1995)]. The figures show upper mantle cross sections under Europe at (A) 100-km and (B) 600-km depth. The white scale bars represent 500 km. The colour scale bar represents the percentage difference in velocity, with the red colours indicating velocities lower than the reference model velocity and the blue colours indicating higher relative velocities. X = 2% in (A), 1% in (B). Even in this evaluation, lower velocities can be identified at a depth of 100 km below parts of the Rhenish Massif, SW Germany and the Bohemian Massif. The deviation is also obvious below the Massif Central, where a mantle plume was detected (Barth et al., 2007). The values at a depth of 600 km show that there is no connection of this low-velocity band to the lower mantle.

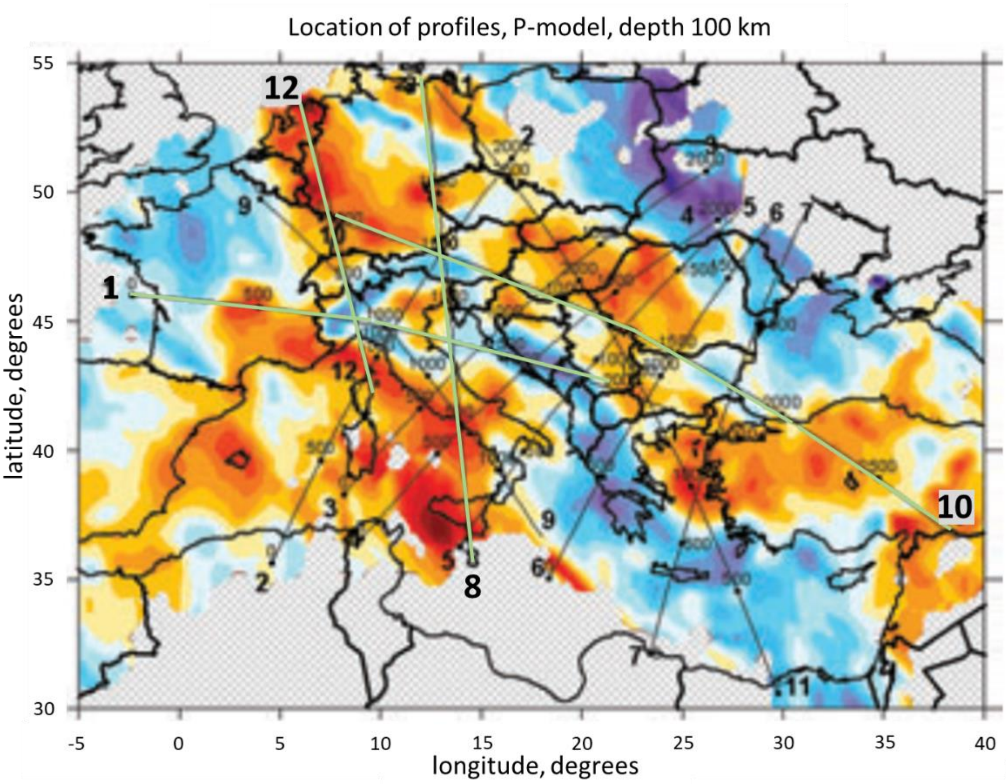

Figure S2 from Koulakov et al. (2009): Position of the profile sections described below (P1, P12, P8, P10) on the horizontal representation of the mantle anomalies (P waves) at a depth of 100 km.

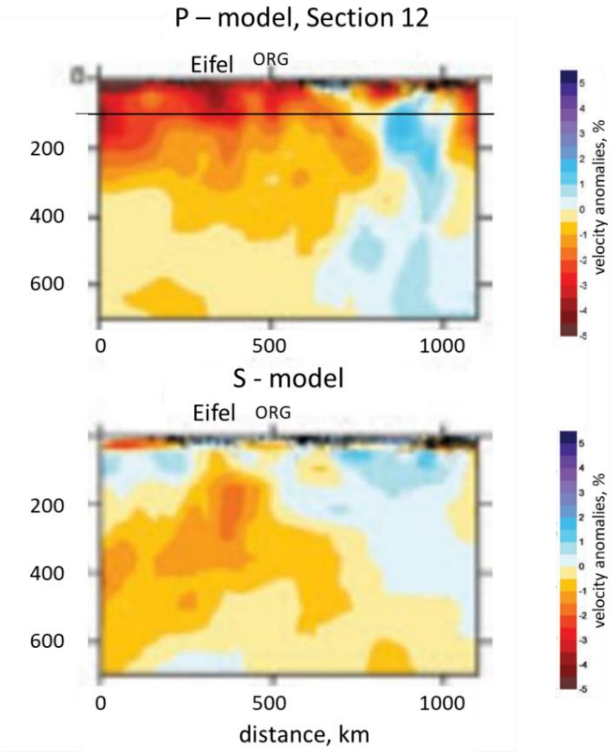

Figure S3 from Koulakov et al. (2009): Vertical section for profile 12 in Figure S2. The NNW-SSE profile shoes the velocity anomaly of P and S waves in the mantle below the Rhenish Massif and SW Germany.

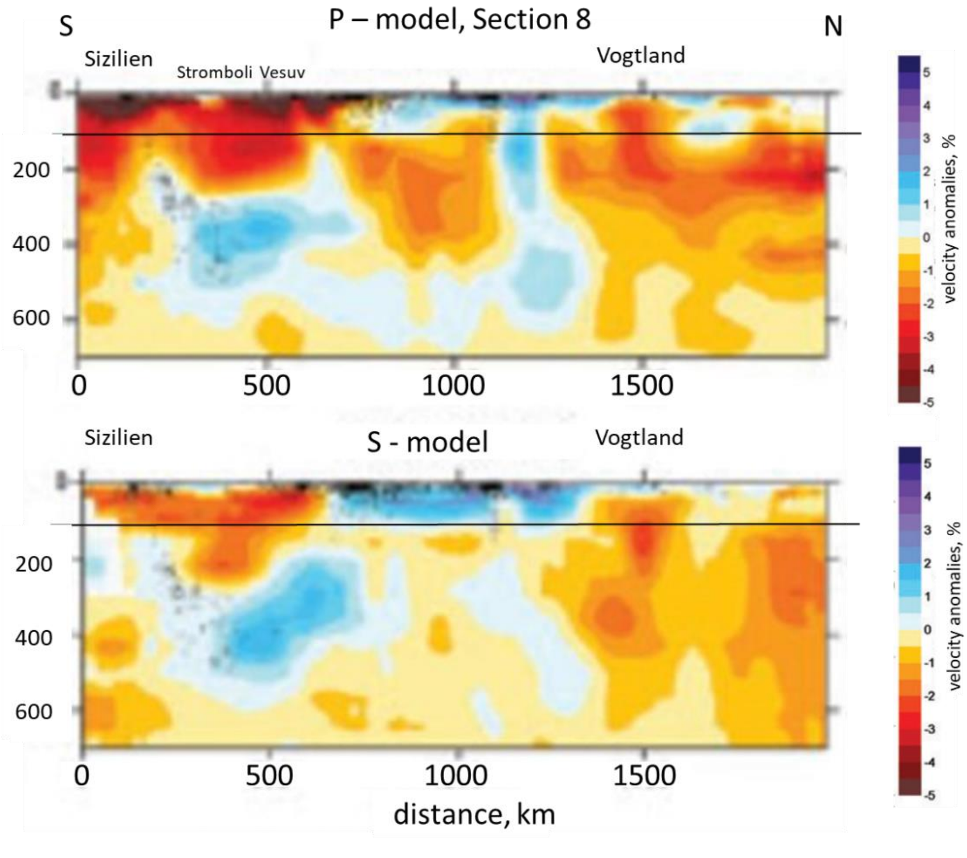

Figure S4 from Koulakov et al. (2009): Profile 8 from Figure S2. S-N profile showing the velocity anomalies of P and S waves in the mantle below the Vogtland.

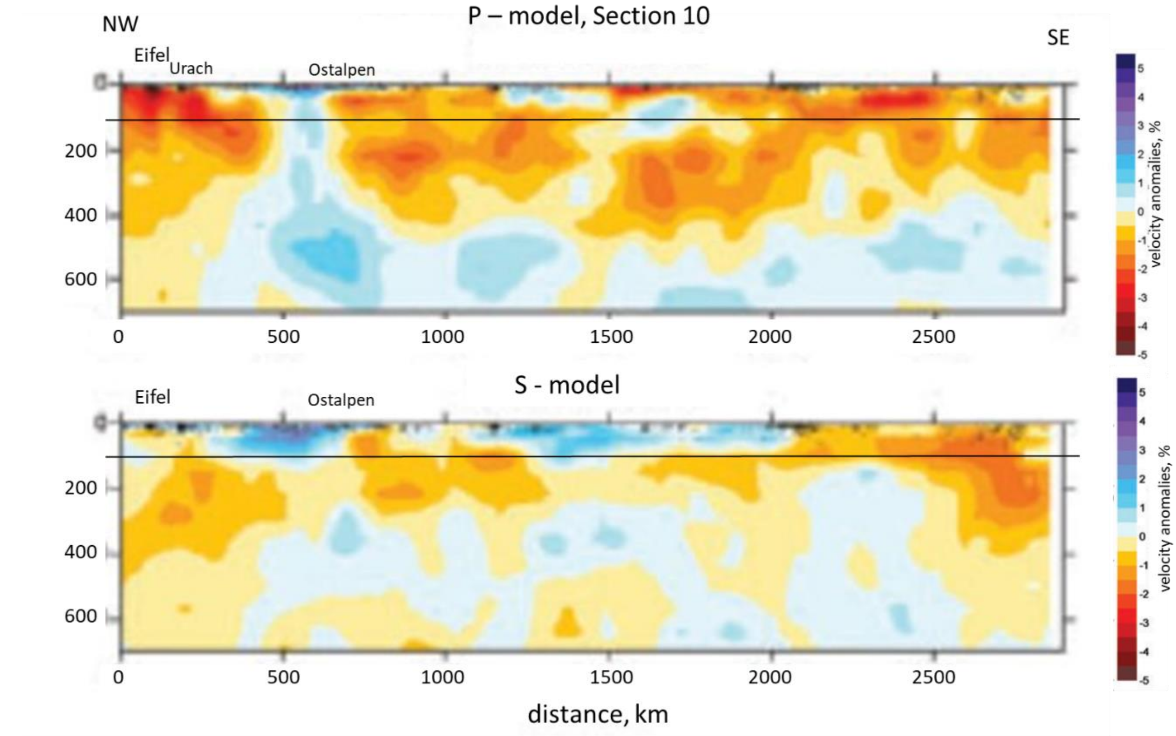

Figure S5 from Koulakov et al. (2009): Profile 10 from Figure S2. NW-SE profile showing the velocity deviations of P and S waves in the mantle below the Rhenish Massif and south Germany.

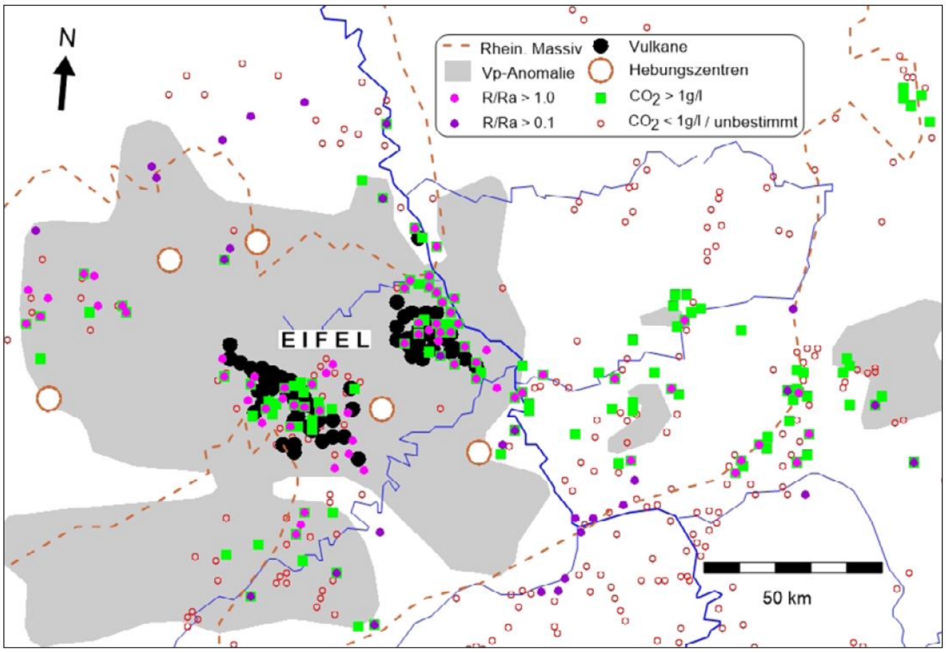

Figure S6 from May (2019): Helium isotope ratios R/Ra in the Rhenish Massif and adjacent areas (light red points R/Ra> 1) as well as CO_2 sources with more than 1g/l (green squares).

Table S1 from Griesshaber et al. (1992): Helium isotope data from the Eifel, Vogelsberg/Taunus region and southern Upper Rhine Valley

Griesshaber et al 1992							
		Gas/Wasser					
Probenahmeorte	Quelle	g/w	R/R_a	Probenahmeorte	Quelle	g/w	R/Ra
Aachen		w	0.21				
Oberrheingraben (Siebengebirge-Osteifel-Neuwieder Becken)				**Hunsrück-Taunus-Vogelsberg, Fortsetzung**			
Köln	Messebrunnen III	g	0.83	Kiedrich	Virchowquelle	w	0.38
Bad Honnef	Drachenquelle	w	2.32	Geisenheim	Echterquelle	w	0.39
Bad Honnef	Edelhof-Stift	g	2.45	Wiesbaden	Faulbrunnen	w	0.63
Bad Honnef	Grafenwerth	g	2.60	Wiesbaden	Kochbrunnen	g	1.00
Bad Neuenahr	Appolinaris No. 10	w	4.21	Wiesbaden	Schützenhofquelle	w	0.70
Bad Neuenahr	Willibrordus	g	4.55	Wiesbaden	Salmquelle	w	0.93
Bad Neuenahr	Walburgis-Therme	g	4.40	Bad Münster	Rheingrafen (süd)	w	0.08
Bad Sinzig	Tiefbrunnen 1	w	1.00	Bad Kreuznach	Quelle No. 5	w	0.09
Bodendorf	Badequelle	g	1.50	Bad Kreuznach	Elisabethquelle	w	0.09
Andernach	Namedy	g	3.61	Bad Kreuznach	Karlshallenquelle	w	0.09
Andernach	Namedy	g	3.61	Krontal	Theodorusquelle	w	2.64
Andernach	Namedy	g	3.61	Bad Soden	Große Bädersprudel	g	2.19
Brohl	Kreyerquelle	g	4.10	Bad Soden	Wilhelmsbrunnen	w	1.78
Wehr	Bohrung 700 m	g	4.95	Bad Homburg	Solesprudel	w	1.48
Wehr	Bohrung 5	g	5.56	Bad Homburg	Augusta-Lech	w	1.56
Wehr	Bohrung 5	w	5.00	Bad Homburg	Elisabeth	w	1.42
Glees	Bohrung 500 m	g	5.00	Bad Nauheim	Sprudel 14	g	0.62
Glees	Bohrung 500 m	w	5.87	Bad Vilbel	Hassia 2	g	3.41
Glees	Bohrung 800 m	g	4.76	Bad Vilbel	Hassia 1	w	3.14
Rieden	Sauerbrunnen	w	5.17	Bad Vilbel	Kad-Friedrich	g	3.17
Bad Hönningen	Deutschland Sprudel	g	4.91	Offenbach	Kaiser Friedrich	w	0.50
Laacher See	CO2 Gas vom See	g	5.40	Selters/Ortenberg	Benedictus	w	0.81
Nickenich	Sauerbrunnen	w	3.82	Schwalheim	Ludwigsbrunnen	g	1.29
Kobern	Belthal Sprudel	g	3.26	Großkarben	Ludwigsquelle	w	1.29
Kobern	Sauerbrunnen	w	1.41	Gelnhausen	Solebohrung	g	0.73
Mühlheim-Kährlich	Sauerbrunnen	g	2.83	Bad Orb	Martinsquelle	w	0.68
Ochtendung	Sauerbrunnen	w	2.51	Bad Salzschlirf	Sprudelbrunnen	w	0.55
Oberzissen	Sauerbrunnen	w	3.81	Giessen	Graf Meinhardt	w	0.73
Winningen	Sauerbrunnen	w	1.51	Selters	Löhnberg	w	1.02
Bassenheim	Sauerbrunnen	w	2.75				
Lahnstein	Victoria	w	1.80	**Kaiserstuhl - Schwarzwald**			
Plaidt	Burquelle	w	3.18	Bad Teinach	Hirschquelle	w	0.10
Mendig	Reginaris	w	0.68	Bad Teinach	Otto-Therme	w	0.10
Rhens	Kaiser Ruprecht	w	1.15	Bad Liebenzell		w	0.01
Bad Ems	borehole III	g	1.55	Baden-Baden	Fettquelle	w	0.02
Bad Ems	borehole I	g	1.57	Baden-Baden	Murgquelle	w	0.10
Bad Salzig	Leonorequelle	w	0.62	Baden-Baden	Ursprungsquelle	w	0.06
Fachingen	HB 9	g	1.60	Bad Herrenalb	Bohrung I	w	0.01
Niederselters	Urselters	g	1.86	Bad Herrenalb	Bohrung II	w	0.04
				Bad Griesbach	Rench 3	w	0.34
				Badenweiler	Römerquelle	w	0.31
Westeifel				Badenweiler	Bohrung III	w	0.43
Wallenborn	Sauerbrunnen	g	3.00	Waldkirsch		w	0.30
Birresborn	Adonisquelle	g	3.10	Bad Bellingen	Bohrung III (2)	g	0.42
Steinborn	Sauerbrunnen	w	3.40	Bad Bellingen	Markusquelle (2)	g	0.43
Gerolstein	Glees Sauerbr. Drees	w	3.30	Bad Bellingen	Bohrung III (1)	w	0.46
Büdesheim	Sauerbrunnen	w	2.43	Bad Bellingen	Markusquelle (1)	w	0.59
Dreis	Marienquelle	g	3.50	Bad Rippoldsau	Bohrung 200 m	w	0.44
Daun	Adelheidquelle	g	4.03	Bad Rippoldsau	Bohrung 300 m	w	0.55
Hunsrück-Taunus-Vogelsberg				Bad Peterstal	Freyersbach	g	0.34
Hardtwald	Sauerbrunnen	w	0.27	Bad Krozingen	Bohrung IV	w	1.73
Schwollen	Diamantenquelle	w	0.23	Freiburg	Thermalbad	g	1.52
Schwollen	Hochwald-Sprudel	w	0.24	Bahlingen	Sauerbrunnen	g	1.30
Gielert	Sauerbrunnen	w	0.30	Grenzach (west)	Emiliane	w	0.38
Bad Schwalbach	Schwalbenbrunnen	w	1.90	Bad Säckingen	Badquelle	w	0.13
Bad Schwalbach	Stahlbrunnen	g	2.10	Baden Limmat		w	0.06
Schlangenbad	Nissenquelle	w	0.54				

Table S2 excerpt from Bräuer et al. (2018): He isotope data from the Vogtland,

Bräuer et. al. 2018			
	Freie Gasphase		
Ort	Quelle	(3He/4He)c /Ra -Wert (Jahr)	älterer Höchstwert (Jahr)
Gasfeld Cheb Becken (CB) und Umgebung			
Dolní Častkov	Mofette	5.28 (2016)	
Bublák	Mofette	5.95 (2016)	
Hartoušov	Mofette	5.60 (2016)	5.74 (2014)
Bad Brambach, Wettinquelle	Quelle	2.36[a] (2014)	
Plesná	Quelle	3.24 (2016)	
Kopanina	Quelle	4.54 (2016)	4.67 (2015)
Cisařský pramen	Quelle	3.38 (2016)	3.43 (1993)
Soos mofette	Mofette	3.50 (2016)	3.55 (2014)
Kyselecký Hamr	Quelle	3.97 (2016)	
Skalná, Nová Ves II	Mofette	5.61 (2014); 5.71 (2007)	5.91 (2006)
Bad Brambach, Eisenquelle	Quelle	2.39 (2015)	
Františkovy Lázně Mariin pramen	Mofette	3.36 (2014)	
Hartoušov (HJB-1)	Borehole	5.75 (2016)	
Hartoušov (1H-031)	Borehole	5.75 (2016)	
Gasfeld Mariánské Lázně (ML) und Umgebung			
Prameny	Quelle	4.60 (2014)	4.87 (1993)
Louka, Grünska kys.	Quelle	4.56 (2014)	
Farska kyselká	Quelle	3.22 (2014)	3.94 (1993)
Smrad'och	Mofette	4.17 (2014)	
ML Mariiny	Mofette	4.08 (2014)	4.73 (1994)
Sirňák, Podhorní Vrch	Mofette	3.53 (2016)	
Čiperka	Quelle	2.93 (2014)	3.32 (1992)
Otročín	Quelle	3.81 (2014)	4.09 (1993)
Křepkovice	Quelle	2.46 (2014)	
Kokašice	Quelle	3.12 (2014)	
Břetisl., Na Hadovce	Quelle	1.89 (2014)	1.90 (1993)
Gasfeld Karlovy Vary (KV)			
Dorotka	Quelle	2.17 (2014)	2.35 (2001)

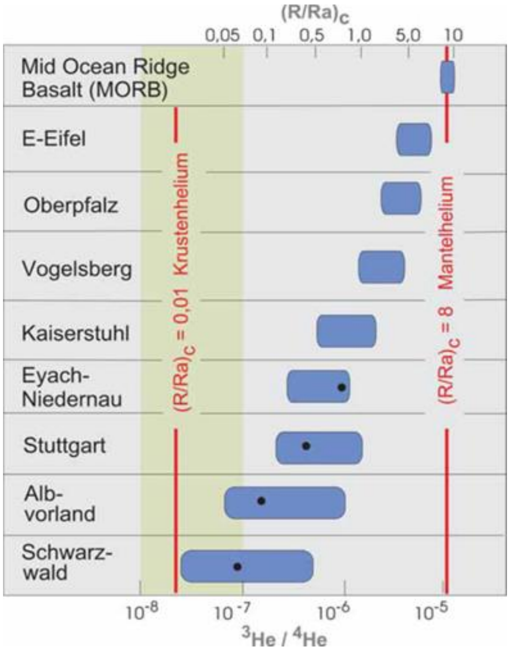

Figure S7 from Ufrecht (2006): Helium isotope values of groundwater in rift zones compared to values of the Stuttgart-Bad Cannstatter and -Berger mineral springs and the foothills of the Alb (Upper Muschelkalk). The blue fields cover the range of the determined 3He/4He isotope ratios or R/Ra values. The black points in the blue fields correspond to the mean 3He/4He isotope ratio in the respective examination area; supplemented after Griesshaber (1992).

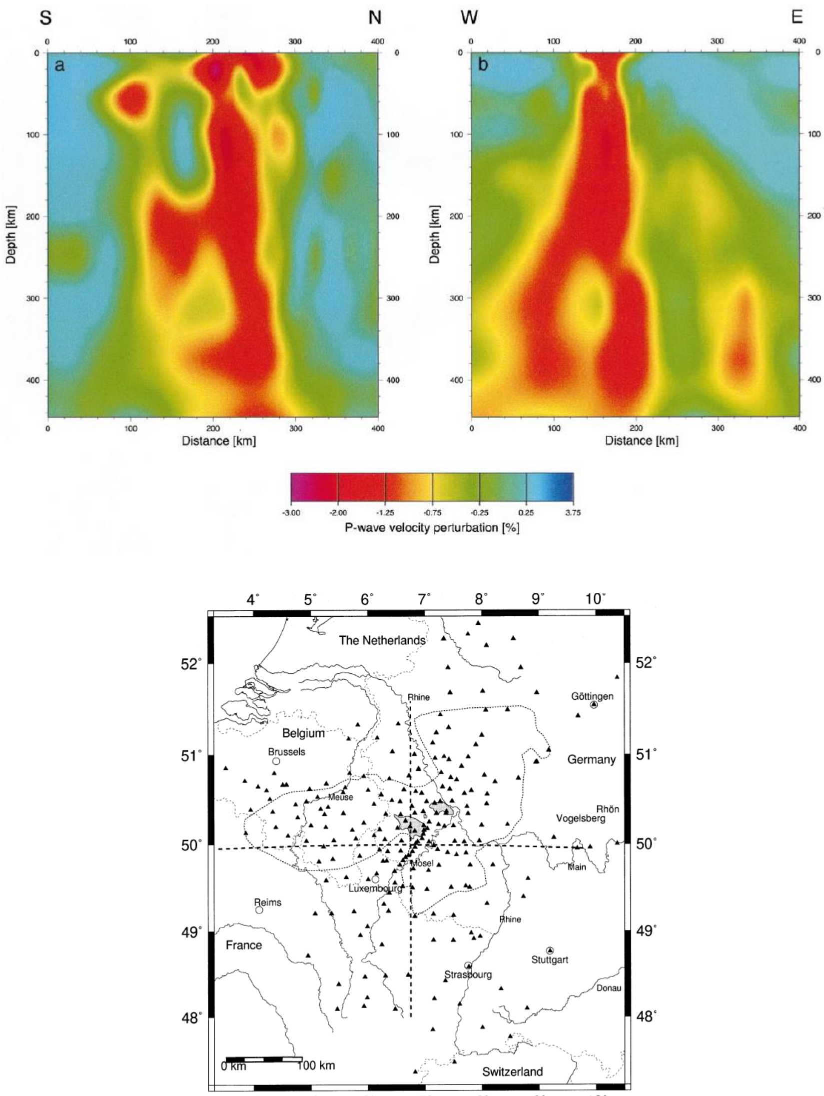

a b

c

Figure S8 from Ritter et al. (2001): Tomographic model of the Eifel Plume in vertical S-N (a) and W-E (b) profile sections. The deviations of the P-wave velocities are shown. The red colours indicate the areas with low seismic velocities for which elevated temperatures are assumed (150 - 200° C). Figure c: position of the profiles. Black triangles indicate the seismic stations used to measure the P-wave velocities.

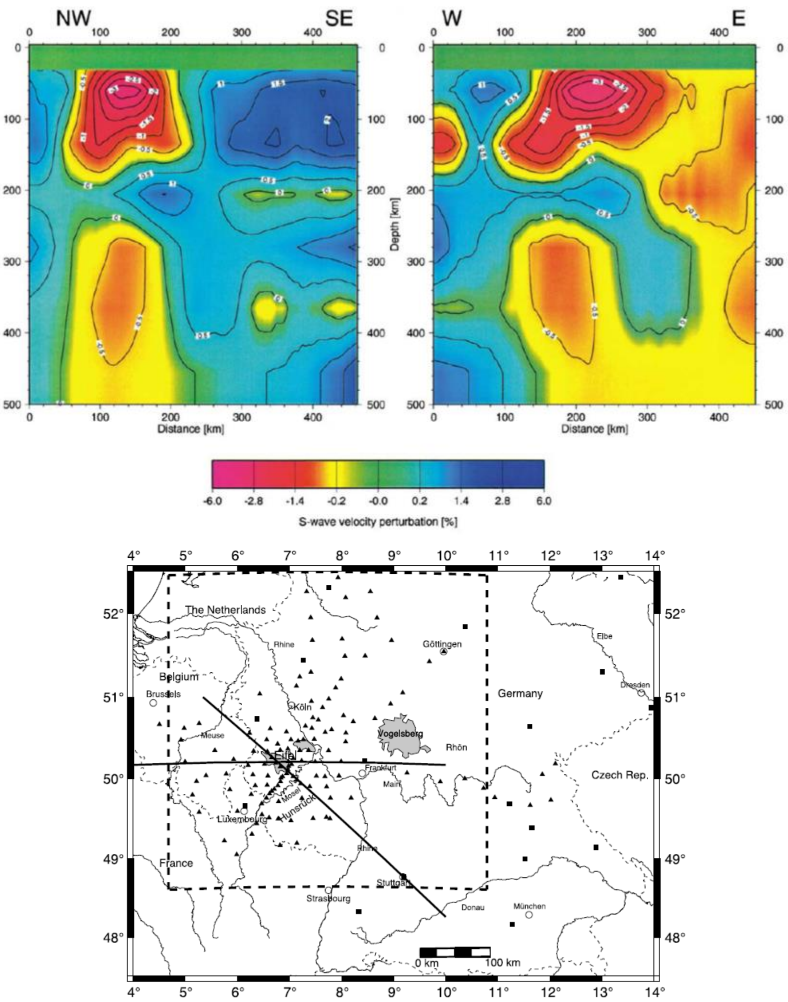

Figure S9 from Keyser et al. (2002): Vertical profile of the tomographic mantle model beneath the Eifel with representation of the shear wave velocity deviation (in color) and map of the positions of the profiles for the tomographic modelling of the Eifel Plume. The triangles denote the positions of the mobile stations, the squares those of the permanent stations that were used for the measurements. The dashed square describes the position of the horizontal sections from Figure S10.

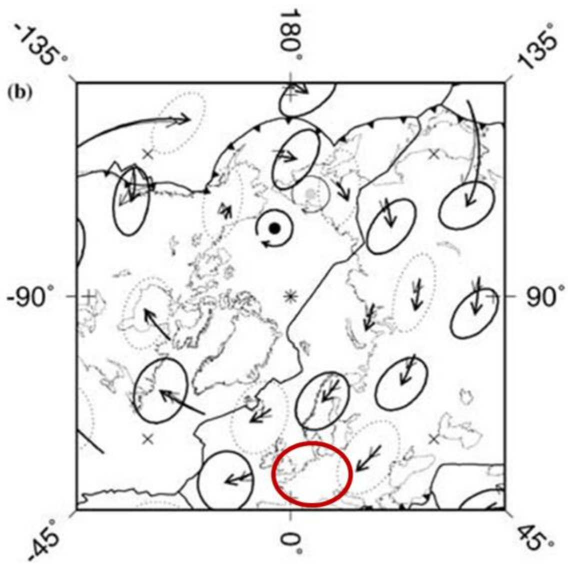

Figure S10 from Gripp and Gordon (2002): Velocities of the Eurasian and North African plates in relation to hotspots. Each arrow shows the displacement path of a point on a plate if the plate were to maintain its current angular velocity relative to the hotspots for 40 Ma. Black ellipses indicate the 2-D 95% confidence interval of velocity, multiplied by 40 million years. The red ellipse shows the location of Central Europe.

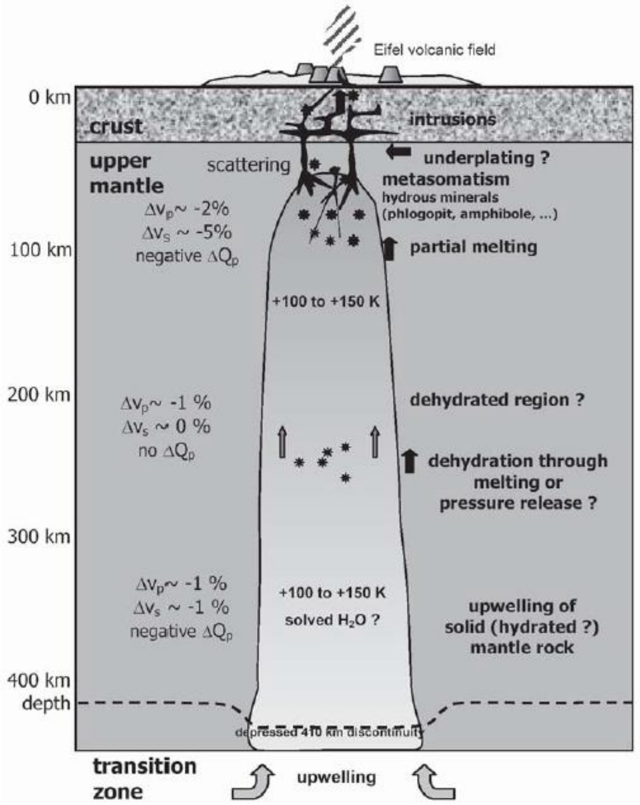

Figure S11 from Ritter (2007): Summarizing schematic representation of the Eifel plume after evaluating the information obtained from various seismological measurements. The lithosphere/asthenosphere boundary is not depicted.

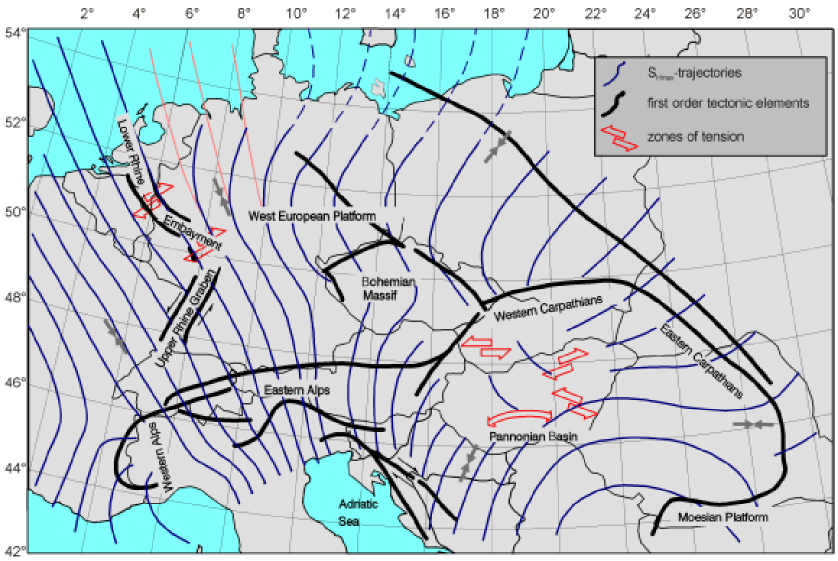

Figure S12 from Grünthal and Stromeyer (1994): Trajectories of the maximum horizontal compressive stress SH_{max} in the crust.

Table S3 from Förster et al. (2019): Age data of various maar tephra layers from drill cores of the Eifel maars compared to tephra ages in other studies.Selection of sampled tephra layers from ELSA drill cores with corresponding approximate ages as proposed by Sirocko et al. (2016).

Tephra	Source:	Depth in core (m)	Core ID	Core location	Age from core (a BP)	Tephra age (literature, a BP)
LST	Laacher See (East Eifel)	13.9	AU2	Auel Maar	12 900*	12 900 (Brauer *et al.*, 1999)
		3.5	DE3	Dehner Maar		
		9.6	HM1	Holzmaar		
		13.6	RM1	Rother Maar		
WBT	Wartgesberg	36.8	**AU2**	Auel Maar	27 900*	30 000 (Sirocko *et al.*, 2013)
		37.8	**DE3**	Dehner Maar		31 000 ± 11 000
		8.8	MS1	Merscheider Maar		(Mertz *et al.*, 2015)
		28.9	RM2	Rother Maar		
DWT	Dreiser–Weiher	71.2	AU2	Auel Maar	41 000*	41 000 (Sirocko *et al.*, 2013)
		47.7	**DE3**	Dehner Maar		
		49.4	**JW3**	Jungferweiher		
		21.5	MS1	Merscheider Maar		
		42.7	RM2	Rother Maar		
		39.5	OW1	Oberwinkler Maar		
MMT	Meerfelder Maar	81.6	AU2	Aueler Maar	43 900*	45 000 (Sirocko *et al.*, 2013)
		50.9	**DE3**	Dehner Maar		
		28.1	MS1	Merscheider Maar		
SMT	Schalkenmehrener Maar	79.6	DE3	Dehner Maar	64 000	–
		79.8	JW2	Jungferweiher		
		80.9	**JW3**			
PMT	Pulvermaar	112.7	**JW3**	Jungferweiher	~75 000	74 000–90 000 (Pouclet *et al.*, 2008)
		11.6	**HL4**	Hoher List Maar		
		21.8	**Ei2**	Eigelbach Maar		
MBT	Mosenberg	120.8	JW2	Jungferweiher	~80 000	80 000 (Zöller and Blanchard, 2009)
		124.6	**JW3**			
		34.3	**HL2**	Hoher List Maar		
		27.3	**HL4**			
		27.3	**Ei2**	Eigelbach Maar		
DMT	Dümpelmaar (East Eifel)	133.3	JW2	Jungferweiher	~106 000	116 000 ± 16 000 (van den Bogaard and
		139.1	**JW3**			Schmincke, 1990)
		41.2	**HL4**	Hoher List Maar		
		34.6	Ei2	Eigelbach Maar		
JWT	Jungferweiher	154.4	**JW3**	Jungferweiher	~136 000	–
		82.2	**HL2**	Hoher List Maar		
		12.9	**WD1**	Walsdorf Maar		

*Dated by ice-core tuning by Sirocko *et al.* (2016). Core ID in bold = sample for EPMA analyses.

Table S4 from Förster and Sirocko (2016): Age of tephra layers in Eifel lake sediments after counting of varves in agreement with ice core data (b2k is the abbreviation for: Before 2000, a point in time based on the year 2000.)

Tephra	Ages in this study	Method	Ages in literature
Laacher See Tephra (LST)	12,900 b2k	From literature	12,900 b2k (Zolitschka, 1998)
Wartgesberg Tephra (WBT)	27,900 ± 2000 b2k	Ice-core tuning (Sirocko et al., this volume)	~20,000 b2k (Eltville tephra, Juvigné and Pouclet, 2009), 31,000 b2k (Pirrung et al., 2007), 30,000 b2k (Sirocko et al., 2013) 31,000 ± 11,000 b2k (Mertz et al., 2015)
Unknown Tephra (UT1)	30,200 ± 2000 b2k	Ice-core tuning (Sirocko et al., this volume)	~28,000 b2k ("Rambach-Wallertheim Tuff", Zöller et al., 1988), 33,000 b2k (Sirocko et al., 2013)
Dreiser Weiher Tephra (DWT)	41,000 ± 2000 b2k	Ice-core tuning (Sirocko et al., this volume)	41,000 b2k (Sirocko et al., 2013)
Unknown Tephra (UT2)	43,900 ± 2000 b2k	Ice-core tuning (Sirocko et al., this volume)	45,000 b2k (Sirocko et al., 2013)
Leucite Tephra (LcT)	~60,000 b2k	Sedimentation rates	–
Dümpelmaar Tephra (DMT)	106,000 b2k	From literature	106,000 b2k (Sirocko et al., 2005) 116,000 ± 16,000 b2k (van den Bogaard and Schmincke, 1990a, 1990b)
Unknown Tephra (UT3)	~140,000 b2k	Sedimentation rates	–
Glees Tephra (GlT)	151,000 b2k	From literature	151,000 ± 11,000 b2k (van den Bogaard and Schmincke, 1990a, 1990b)
Hüttenberg Tephra (HBT)	215,000 b2k	From literature	215,000 ± 4000 b2k (van den Bogaard et al., 1989)

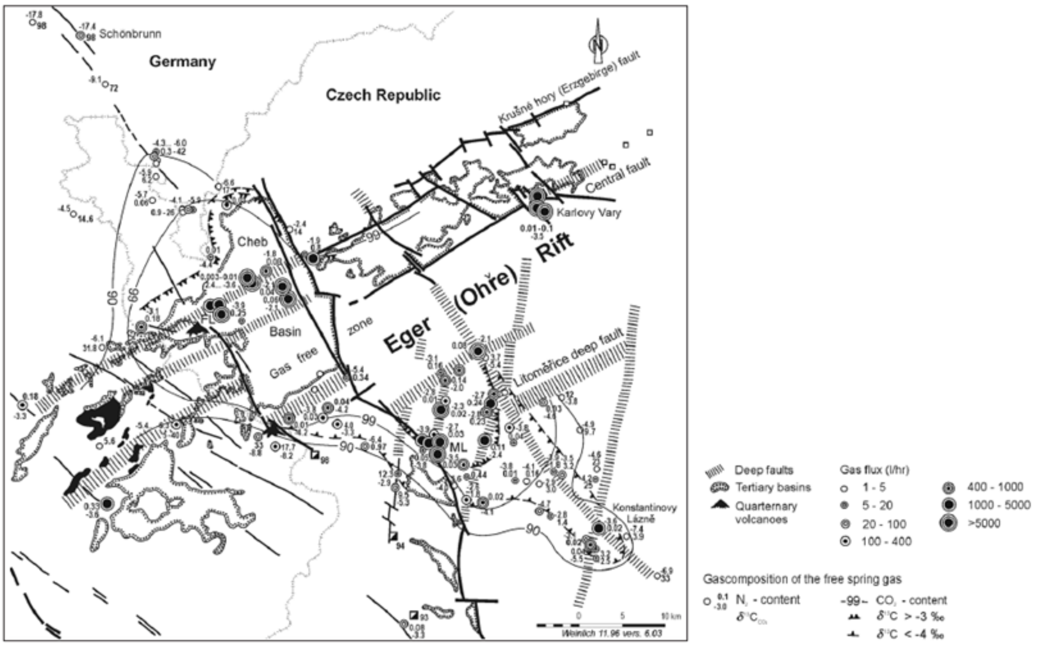

Figure S13 from Weinlich (2005): Distribution pattern of the gas escape points in the vicinity of the Eger rift along deep-reaching fault zones as well as $\delta^{13}C_{CO2}$ values of the gases in mineral springs and mofettes (data from Weinlich et al., 1998, 1999, 2003). ML - Mariánské Lázne, Marienbad; FL - Frantiskovy Lázne, Franzensbad; Karlovy Vary - Carlsbad.

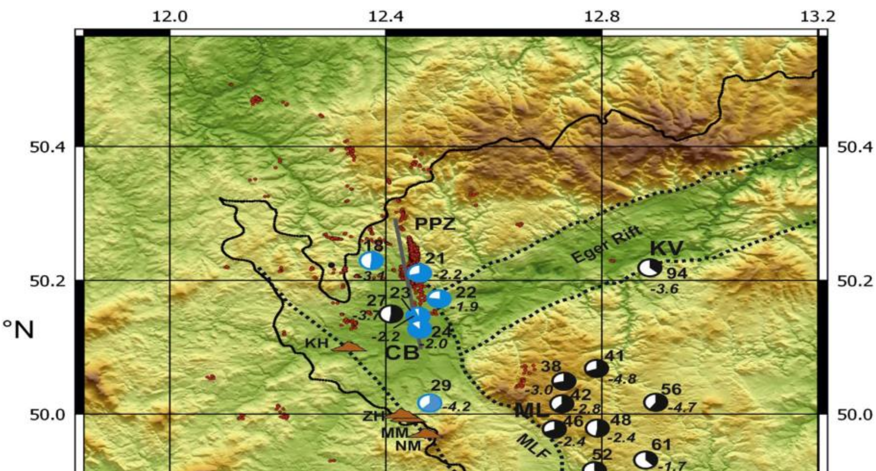

Figure S14 from Bräuer et al. (2018): Overview of the degassing centres of the Eger Basin and the area around Marienbad (Mariánské Lázně, ML) and Potočky–Plesná Fault Zone (PPZ) with the analysed mofettes and springs. The black and blue sectors show the mantle-born helium fractions. The black ones indicate the places where the fraction of the mantle helium has remained about the same while the blue ones indicate the places where this proportion has strongly increased. Large numbers: sample numbers, small negative numbers: $\delta^{13}C$ values; KV - Karlovy Vary.

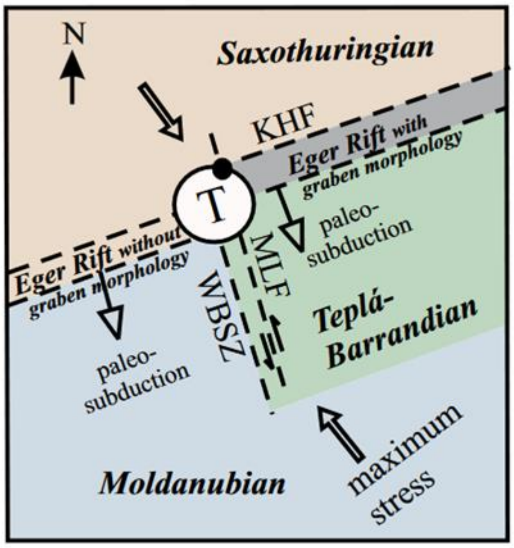

Figure S 15 from Babuška and Plomerová (2010): Tectonic sketch showing the location of the Cheb Basin at the triple (T) point of three mantle-lithospheric domains, which probably correspond to remnants of three microplates that had collided during the Variscan orogeny. The northwestern area of the Tepla-Barrandium microplate is the most active part of the Bohemian Massif, which includes the Nový Kostel earthquake swarm zone (black dot). MLF: Mariánské Lázně Fault, KHF: Krušné Hory Fault, WBSZ: West Bohemian Shear Zone.

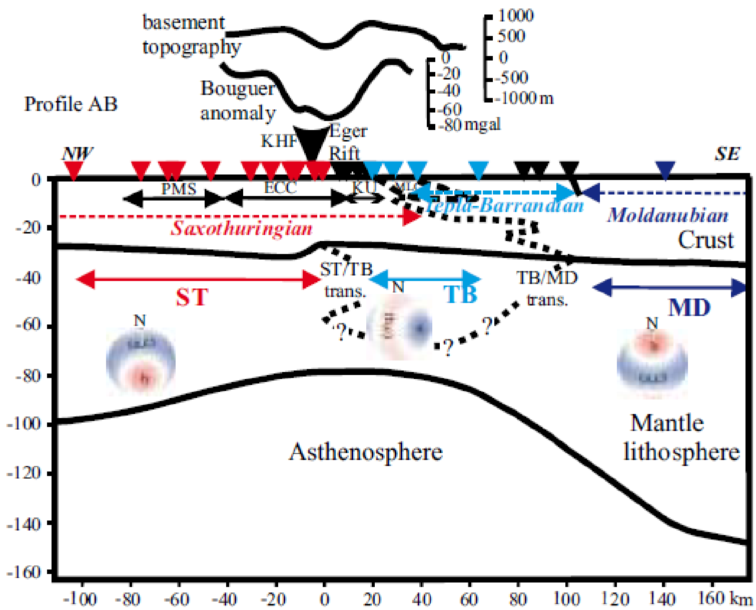

Figure S16 from Babuška and Plomerová (2010): NW – SE cross-section (trace see Figure S17) through the eastern part of the Cheb Basin. Bulging of the asthenosphere to -80 km and the crust-mantle boundary under the Eger Rift to - <28 km. KHF: Krusne hory fault, PMS: Paleozoic metasediments, ECC: Erzgebirge crystalline complex, TCC: Tepla crystalline complex, KU: Kladska unit, MLC: Marianske Lazne Complex.

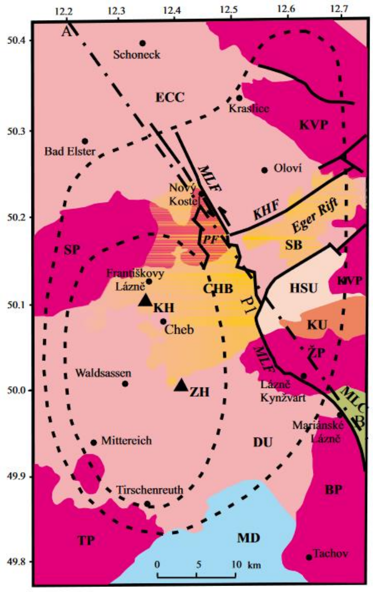

Figure S 17 from Babuška and Plomerová (2010): Simplified geological map of the three amalgamated lithospheric blocks Saxothuringian, Tepla Barandian and Moldanubian in the Vogtland. Saxothuringian: ECC – Krušné hory Crystalline Complex, DU – Dyleň Unit, HSU – Horní Slavkov Unit, KU – Kladská Unit; Teplá-Barrandian: MLC – Mariánské Lázně Complex; MD—Moldanubian. Variscan granitoids: SP – Smrčiny (Fichtelgebirge) pluton, KVP – Karlovy Vary pluton, ŽP – Žandov pluton, BP – Bor pluton, TP – Tirschenreuth pluton. CHB – Cheb Basin, SB – Sokolov Basin. KHF - Krušné Hory Fault, MLF - Mariánské Lázně Fault, PF - Plesná Fault (Schunk et al. 2003). Quaternary volcanoes: KH – Komorní hůrka and ZH – Železná hůrka. The dashed lines show the thinning of the crust: outer line 30 km and inner line 28 km below the Cheb Basin (Heuer, 2006).

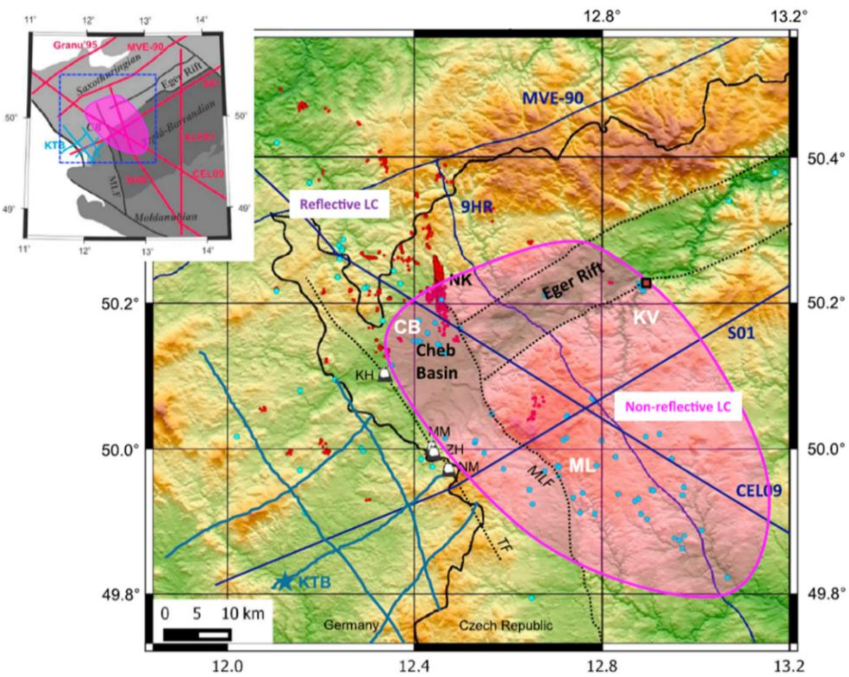

Figure S18 from Hrubcova et al. (2017): Surface projection of a Late Cenozoic magmatic body in the lower crust as a result of underplating, derived from non-reflective LC seismic data, gas geochemistry and volcanic activity. Epicentres of local earthquake swarms from 1995 - 2015 are shown as red dots (Bouchaala et al., 2013), blue dots represent localities of gases escaping at the surface (Geissler et al., 2005). Blue lines indicate the traces of the seismic refraction or reflection profiles. Volcanoes: KH, Komorní hůrka; ZH, Železná hůrka; MM, Mytina Maar; NM, Neualbenreuth Maar. Fault zones: MLF, Mariánské Lázně Fault; TF, Tachov Fault. The overview map shows the position of the magmatic body in relation to tectonic units of the Variscides in western Bohemia. The Quaternary volcanoes lie on the postulated Tachov fault, so it can be assumed that the fault path favoured the ascent of the magmas. It is striking that the volcanically active zone lies outside the surface projection of the postulated intrusive body.

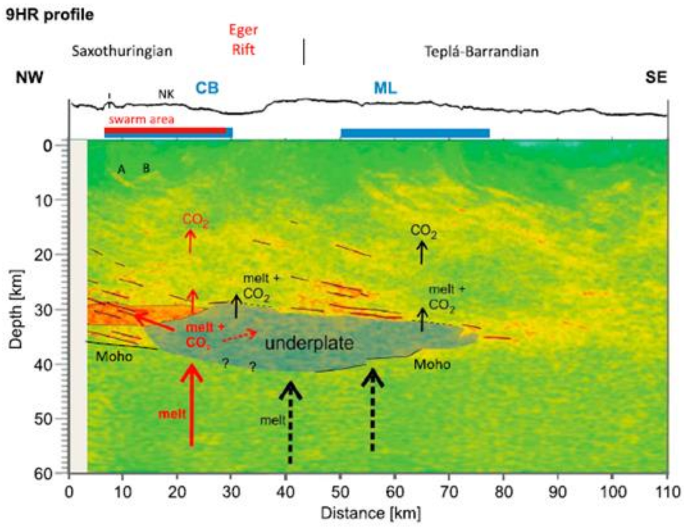

Figure S19 from Hrubcova et al. (2017, profile 9HR from Figure S18, Suppl.). The postulated magmatic body is depicted as "underplate", its emplacement has been proposed to have occurred in the late Cenozoic. The red arrows outline possible paths of magmas and gases as part of active magmatic activity. Black arrows show recent activity, dashed arrows past activity. The blue bars show the extent of the gas escape centres at the surface CB (Cheb Basin) and ML (Mariánské Lázně), the red bar shows the region of the earthquake swarms near Nový Kostel (NK).

References

Babuška, V. and Plomerová, J.: Mantle lithosphere control of crustal tectonics and magmatism of the western Ohře (Eger) Rift, J. Geosci., 55, 171–186, https://doi.org/10.3190/jgeosci.066, 2010.
Barth, A., Jordan, M., and Ritter, J. R. R.: Crustal and upper mantle structure of the French Massif Central plume, in: Mantle Plumes – A Multidisciplinary Approach, edited by: Ritter, J. R. R. and Christensen, U. R., Springer, 159–184, https://doi.org/10.1007/978-3-540-68046-8_7, 2007.
Bogaard, P. v. d., Hall, C. M., Schmincke, H.-U., and York, D.: Precise single-grain 40Ar/39Ar dating of a cold to warm climate transition in Central Europe, Nature, 342, 523–525, https://doi.org/10.1038/342523a0, 1989.
Bogaard, P. v. d. and Schmincke, H.-U.: Die Entwicklungsgeschichte des Mittelrheinraumes und die Eruptionsgeschichte des Osteifel-Vulkanfeldes, in: Rheingeschichte zwischen Mosel und Maas, edited by: Schirmer, W., Dtsch. Quartärver., Hannover, 166–190, 1990b.
Bräuer, K., Kämpf, H., Niedermann, S., and Strauch, G.: Indications for the existence of different magmatic reservoirs beneath the Eifel area (Germany): A multi-isotope (C, N, He, Ne, Ar) approach, Chem. Geol., 356, 193–208, https://doi.org/10.1016/j.chemgeo.2013.08.016, 2013.
Bräuer, K., Kämpf, H., Niedermann, S., and Strauch, G.: Monitoring of helium and carbon isotopes in the western Eger Rift area (Czech Republic): relationships with the 2014 seismic activity and indications for recent (2000–2016) magmatic unrest, Chem. Geol., 482, 131–145, https://doi.org/10.1016/j.chemgeo.2018.02.017, 2018.
Brauer, A., Endres, C., and Negendank, J. F. W.: Lateglacial calendar year chronology based on annually laminated sediments from Lake Meerfelder Maar, Germany, Quaternary Int., 61, 17–25, https://doi.org/10.1016/S1040-6182(99)00017-9, 1999.
Förster, M. W. and Sirocko, F.: The ELSA tephra stack: volcanic activity in the Eifel during the last 500,000 years, Global Planet. Change, 142, 100–107, https://doi.org/10.1016/j.gloplacha.2016.05.002, 2016.
Förster, M. W., Zemlitskaya, A., Otter, L. M., Buhre, S., and Sirocko, F.: Late Pleistocene Eifel eruptions: insights from clinopyroxene and glass geochemistry of tephra layers from Eifel Laminated Sediment Archive sediment cores, J. Quaternary Sci., 35, 186–198, https://doi.org/10.1002/jqs.3134, 2019.
Geissler, W. H., Kämpf, H., Kind, R., Bräuer, K., Klinge, K., Plenefisch, T., Horálek, J., Zednik, J., and Nehybka, V.: Seismic structure and location of a CO2 source in the upper mantle of the western Eger Rift, Tectonics, 24, TC5001, https://doi.org/10.1029/2004TC001672, 2005.
Goes, S., Spakman, W., and Bijwaard, H.: A lower mantle source for Central European volcanism, Science, 286, 1928–1931, https://doi.org/10.1126/science.286.5446.1928, 1999.
Griesshaber, E., O'Nions, R. K., and Oxburgh, E. R.: Helium and carbon isotope systematics in crustal fluids from the Eifel, the Rhine Graben and Black Forest, F.R.G., Chem. Geol., 99, 213–235, https://doi.org/10.1016/0009-2541(92)90018-H, 1992.
Gripp, A. E. and Gordon, R. G.: Young tracks of hotspots and current plate velocities, Geophys. J. Int., 150, 321–361, https://doi.org/10.1046/j.1365-246X.2002.01702.x, 2002.

Grünthal, G. and Stromeyer, D.: The recent crustal stress field in Central Europe: trajectories and finite element modelling, J. Geophys. Res., 99, 18005–18020, https://doi.org/10.1029/94JB00128, 1994.
Heuer, B., Geissler, W. H., Kind, R., and Kämpf, H.: Seismic evidence for asthenospheric updoming beneath the western Bohemian Massif, central Europe, Geophys. Res. Lett., 33, L05311, https://doi.org/10.1029/2005GL025158, 2006.
Hrubcová, P., Hrubec, J., Mrlina, J., Bouchaala, F., and Fischer, T.: Fault zone structure and triggering mechanisms of earthquake swarms along the Eger Rift (Czech Republic), J. Geophys. Res.-Sol. Ea., 122, 3159–3176, https://doi.org/10.1002/2016JB013666, 2017.
Keyser, M., Ritter, J. R. R., and Wenzel, F.: Shear wave anomalies beneath the Eifel area and their relation to the Eifel plume, Int. J. Earth Sci., 91, 1034–1048, https://doi.org/10.1007/s00531-002-0277-0, 2002.
Koulakov, I., Kaban, M. K., Tesauro, M., and Cloetingh, S. A. P. L.: P- and S-velocity anomalies in the upper mantle beneath Europe from tomographic inversion of ISC data, Geophys. J. Int., 179, 345–366, https://doi.org/10.1111/j.1365-246X.2009.04279.x, 2009.
May, F.: Möglichkeiten der Prognose zukünftiger vulkanischer Aktivität in Deutschland – Kurzbericht zur Standortauswahl, Bundesanstalt für Geowissenschaften und Rohstoffe (BGR), Hannover, 2019.
Ritter, J. R. R., Jordan, M., Christensen, U. R., and Achauer, U.: A mantle plume below the Eifel volcanic fields, Germany, Earth Planet. Sc. Lett., 186, 7–19, https://doi.org/10.1016/S0012-821X(01)00215-8, 2001.
Ritter, J. R. R.: Subduction, plumes and the structure of the mantle beneath Europe, in: Mantle Plumes – A Multidisciplinary Approach, edited by: Ritter, J. R. R. and Christensen, U. R., Springer, 19–44, https://doi.org/10.1007/978-3-540-68046-8_2, 2007.
Ufrecht, W.: Untersuchung der geochemischen Signale (He-Isotope) im Grundwasser und deren Herkunft in Süddeutschland, Dissertation, Universität Stuttgart, 2006.
Weinlich, F. H.: Isotopically light carbon dioxide in nitrogen-rich gases: the gas distribution pattern in the French Massif Central, the Eifel and the western Eger Rift, Ann. Geophys., 48, 19–31, http://hdl.handle.net/2122/877, 2005.